Experimental and Molecular Pathology 91 (2011) 614–621

Contents lists available at ScienceDirect

Experimental and Molecular Pathology

journal homepage: www.elsevier.com/locate/yexmp

Imaging mass spectrometry analysis reveals an altered lipid distribution pattern in the tubular areas of hyper-IgA murine kidneys

Yukihiro Kaneko [a,*], Yoko Obata [b], Tomoya Nishino [b], Hiroshi Kakeya [b], Yoshitsugu Miyazaki [a], Takahiro Hayasaka [c], Mitsutoshi Setou [c], Akira Furusu [b], Shigeru Kohno [b]

[a] Department of Chemotherapy and Mycoses, National Institute of Infectious Disease, Toyama 1-23-1, Shinjuku-ku, Tokyo 162-8640, Japan
[b] Department of Molecular Microbiology and Immunology, Nagasaki University Graduate School of Biomedical Sciences, 1-7-1 Sakamoto, Nagasaki 852-8501, Japan
[c] Department of Cell Biology and Anatomy, Hamamatsu University School of Medicine, 1-20-1 Handayama, Higashi-ku, Hamamatsu, Shizuoka 431-3192, Japan

ARTICLE INFO

Article history:
Received 7 July 2011
Available online xxxx

Keywords:
Imaging mass spectrometry
Phosphatidylcholine
Urine
Lipid
IgA
Nephropathy
Urinary stagnation
Molecular distribution
Molecular imaging
Deposition

ABSTRACT

Immunoglobulin A (IgA) nephropathy is the most common glomerular disease worldwide. To investigate the pathogenesis of this renal disease, we used animal models that spontaneously develop mesangioproliferative lesions with IgA deposition, which closely resemble the disease in humans. We analyzed the molecular distribution of lipids in hyper-IgA (HIGA) murine kidneys using matrix-assisted laser desorption/ionization-quadrupole ion trap-time of flight (MALDI-QIT-TOF)-based imaging mass spectrometry (IMS), which supplies both spatial distribution of the detected molecules and allows identification of their structures by their molecular mass signature. For both HIGA and control (Balb/c) mice, we found two phosphatidylcholines, PC(16:0/22:6) and PC(18:2/22:6), primarily located in the cortex area and two triacylglycerols, TAG(16:0/18:2/18:1) and TAG(18:1/18:2/18:1), primarily located in the hilum area. However, several other molecules were specifically seen in the HIGA kidneys, particularly in the tubular areas. Two HIGA-specific molecules were O-phosphatidylcholines, PC(O-16:0/22:6) and PC(O-18:1/22:6). Interestingly, common phosphatidylcholines and these HIGA-specific ones possess 22:6 lipid side chains, suggesting that these molecules have a novel, unidentified renal function. Although the primary structure of the HIGA-specific molecules corresponding to *m/z* 854.6, 856.6, 880.6, and 882.6 remained undetermined, they shared similar fragmentation patterns, indicating their relatedness. We also showed that all the HIGA-specific molecules were derived from urine, and that artificial urinary stagnation—due to unilateral urethral obstruction—caused HIGA-specific distribution of lipids in the tubular area.

Introduction

Histopathological findings have provided a significant amount of information on nephropathies and have been used to solve their underlying mechanisms, such as IgA deposition in IgA nephropathy (Muda et al., 1995). In recent years, the emergence of molecular imaging techniques such as green fluorescent protein labeling and immunohistochemistry have expanded the practical applications available to researchers (Drummond and Allen, 2008; Grunkin et al., 2011). Although the techniques for histopathology have been useful in investigating the morphology and distribution of various defects in tissues, conventional techniques such as electron microscopy have failed to identify low-molecular-weight compounds. Moreover, while new systematic approaches (e.g., proteomics and metabolomics using mass spectrometry (MS)) have enabled the identification of various kinds of molecular species and have contributed to a more detailed understanding of the etiology of the disease, as well the discovery of new biomarkers (Baronas et al., 2007; Mimura et al., 1996; Yasuda et al., 2006; Yoshioka et al., 2009; Zhang et al., 2008), these approaches lose the distributional information.

Matrix-assisted laser desorption/ionization-quadrupole ion trap-time of flight (MALDI-QIT-TOF)-based imaging mass spectrometry (IMS) is a technique that supplies both the spatial distribution of the detected molecules and allows the identification of their structures by their molecular mass signature. More recently, the resolution of MALDI-QIT-TOF-IMS has been refined to microscopic level, thereby enabling an analysis of microscopic lesions that conventional approaches have not been able to easily examine (Setou and Kurabe, 2011). Willems et al. recently reported the usefulness of the IMS technology for grading myxoid sarcoma by clustering of the biomolecular signatures in particular lipid compositions (Willems et al., 2010).

The relationship between lipid composition and kidney diseases is not well understood. Hence, we investigated the distribution of lipid compositions in the kidneys of HIGA mice—well-recognized murine

* Corresponding author at. Fax: +81 3 5285 1272.
E-mail address: ykaneko@nih.go.jp (Y. Kaneko).

0014-4800/$ – see front matter © 2011 Elsevier Inc. All rights reserved.
doi:10.1016/j.yexmp.2011.07.002

model for IgA nephropathy (Muso et al., 1996)—using MALDI-QIT-TOF-IMS and analyzed the physiological significance of the molecules detected by it.

Materials and methods

Chemicals

All general chemicals used in this study were purchased from Wako Chemicals (Tokyo, Japan), unless otherwise indicated, and were of the highest purity available. Ultra pure water dispensed by a Milli-Q water system (Millipore, Bedford, MA, USA) was used for the preparation of buffers and solvents.

Animals and sample preparation

All the experiments on the mice were conducted according to the protocols approved by the Animal Care and Use Committee, Nagasaki University, School of Medicine. Kidneys were obtained from 28-week-old Balb/c mice and HIGA mice (Charles River Japan, Kanagawa, Japan), and urine was collected in a cage designed to prevent feces–urine contact (Nalge Nunc International, Tokyo, Japan), as previously described (Kurashige et al., 2008). The tissue samples and urine were immediately frozen and stored at −80 °C until use.

Tissue slice preparation

Tissue slice preparation for imaging mass spectrometry was performed as previously described (Hayasaka et al., 2008; Sugiura and Setou, 2009). Briefly, the frozen intact tissues were sectioned at −20 °C in a cryomicrotome (CM 3050; Leica Microsystems, Wetzlar, Germany) to obtain 5-μm-thick sections, and the frozen slices were then thaw-mounted on indium tin oxide (ITO)-coated glass slides (Bruker Daltonics, Leipzig, Germany). Matrix was coated on the slices by spraying them with 100 μl of 2,5-dihydroxybenzoic acid (Bruker Daltonics) solution (50 mg/ml in 70% methanol/0.1% trifluoroacetic acid) using a 0.2-mm nozzle caliber airbrush (Procon Boy FWA Platinum; Mr. Hobby, Tokyo, Japan). After drying, the ITO slide was adhered to a mass spectrometer target plate with double-sided conductive adhesive tape to facilitate electrical conduction. Positional information for each section was obtained by scanning the section with a chemical inkjet printer CHIP-1000 (Shimadzu Corporation, Kyoto, Japan) prior to MALDI-QIT-TOF-MS analysis.

Extraction of lipids from tissue and urine

Tissues were crudely ground using clean spatulas and further shredded using a sonicator in an approximately 20-fold volume of chloroform-methanol (2:1) in glass tubes on ice. The mixture was

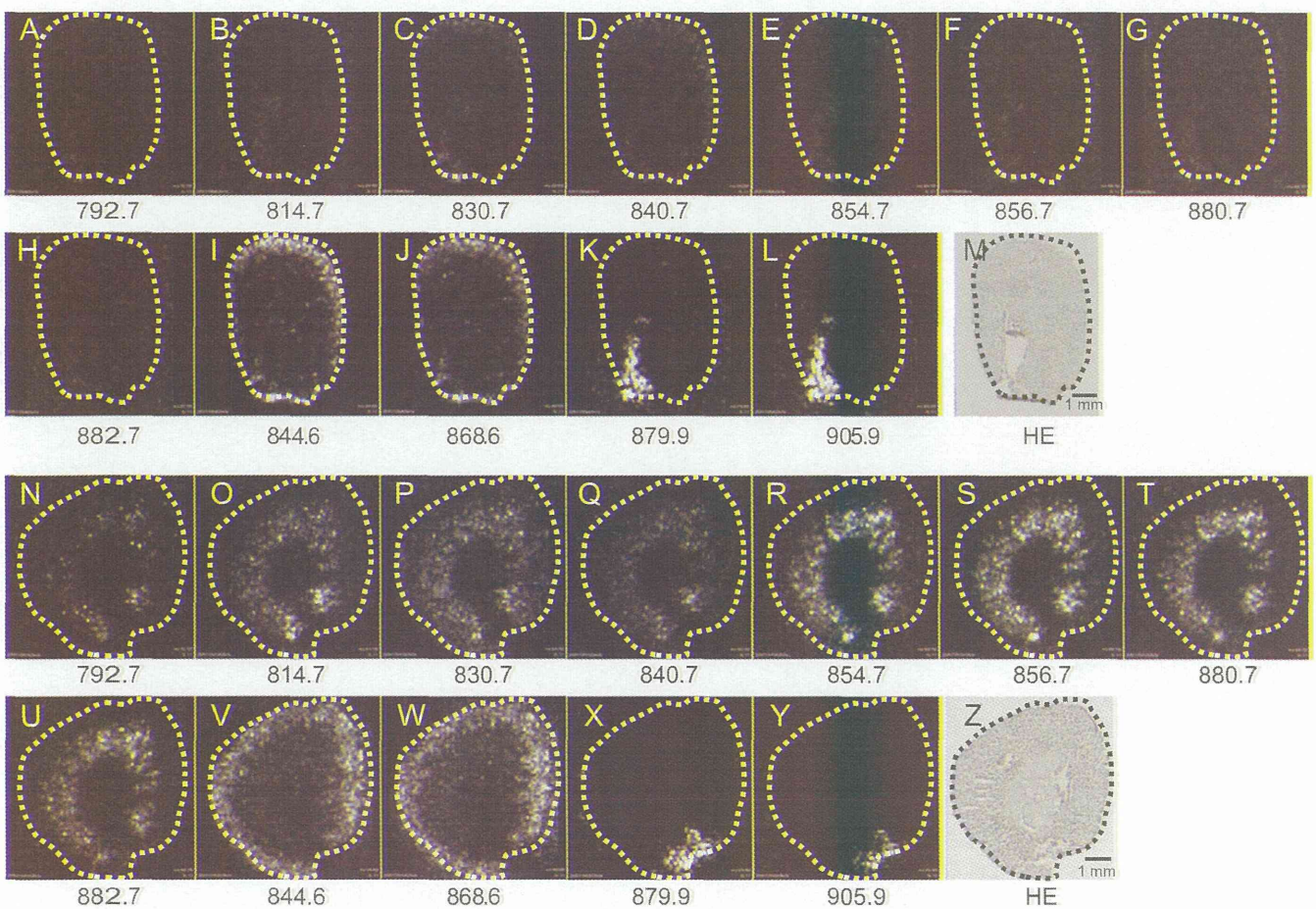

Fig. 1. Eight mass peaks are dominant in the kidneys of HIGA mouse in mass images of kidneys. Significant peaks, *m/z* 792.6, *m/z* 814.6, *m/z* 830.6, *m/z* 840.6, *m/z* 854.6, *m/z* 856.6, *m/z* 880.6, and *m/z* 882.6, are detected in HIGA kidneys (N–U), but absent in the control (A–H). However, 2 significant mass peaks are seen in the peripheral (cortex) area (I,J,V,W), and 2 other significant mass peaks are seen in the hilum area (K,L,W,Y) in both HIGA and control kidneys. The corresponding HE images of the control (M) and HIGA (Z) are also shown. Scale bars indicate a length of 1 mm.

centrifuged at 3000 rpm for 5 min at 4 °C. The supernatant was collected and evaporated, and the dried sample was used for further extraction by the Bligh and Dyer (BD) method (Bligh and Dyer, 1959). Briefly, to 1 ml of the original volume of supernatant, 0.08 ml of water and 0.3 ml of chloroform/methanol (1:2) were added and mixed. Next, 0.1 ml of chloroform was added and mixed, followed by the adding and mixing of 0.1 ml of water. The suspension was then centrifuged at 3000 rpm for 5 min at 4 °C. The organic phase was collected and evaporated, and then reconstituted in appropriate volume of methanol.

Extraction from urine was also performed by the BD method. Briefly, 0.3 ml of chloroform/methanol (1:2) was added to 0.08 ml of urine, and the extraction was performed as above.

These extracted samples were then used for MALDI-QIT-TOF-MS or liquid chromatography-linear ion trap quadrupole-Orbitrap-MS (LC-LTQ-Orbitrap-MS).

Unilateral urethral obstruction

For allowing urine to stagnate, 28-week-old Balb/c mice received unilateral urethral obstruction (UUO), as previously described (Li et al., 2010). Briefly, the left mid-ureter was obstructed by two-point ligations with silk sutures. The mice were sacrificed 2 weeks later.

MALDI-QIT-TOF-MS

All analyses were performed in positive ion mode and in mid-mass range by using a MALDI-QIT-TOF-type mass spectrometer (AXIMA-QIT; Shimadzu Corporation and Kratos Analytical, Manchester, UK), equipped with a 337 nm nitrogen laser, as previously described (Hayasaka et al., 2008; Sugiura and Setou, 2009). An external calibration method was performed with ions from angiotensin II and its decomposition products covering from *m/z* 680 to 900.

Data acquisition and imaging

The data acquisition and processing were controlled by Launchpad software (Kratos Analytical). All the spectra were recorded with the standard instrument settings for optimum transmission. Each raster scan was performed in square regions of 5000 μm to 8000 μm with a measurement pitch of 100 μm automatically. Laser irradiation consisted of 10 shots in each spot, and the power setting was 50 to 60 as appropriate. The raw data were converted by using free software (Axima2Analyze; Novartis, Basel, Switzerland), to apply the BioMap (Novartis). Mass signals between *m/z* 600 and *m/z* 1000 were analyzed with an interval of 0.1 and a tolerance of 0.05, resulting in 4001 images for each experiment. The ion image highlighted the signal intensity obtained from a specific molecule.

Tandem MS analysis

The instrument settings were changed to correspond to the ions from the molecules of interest. The power and collision-induced dissociation (CID) settings were adjusted from 50 to 60 and from 200 to 400, respectively.

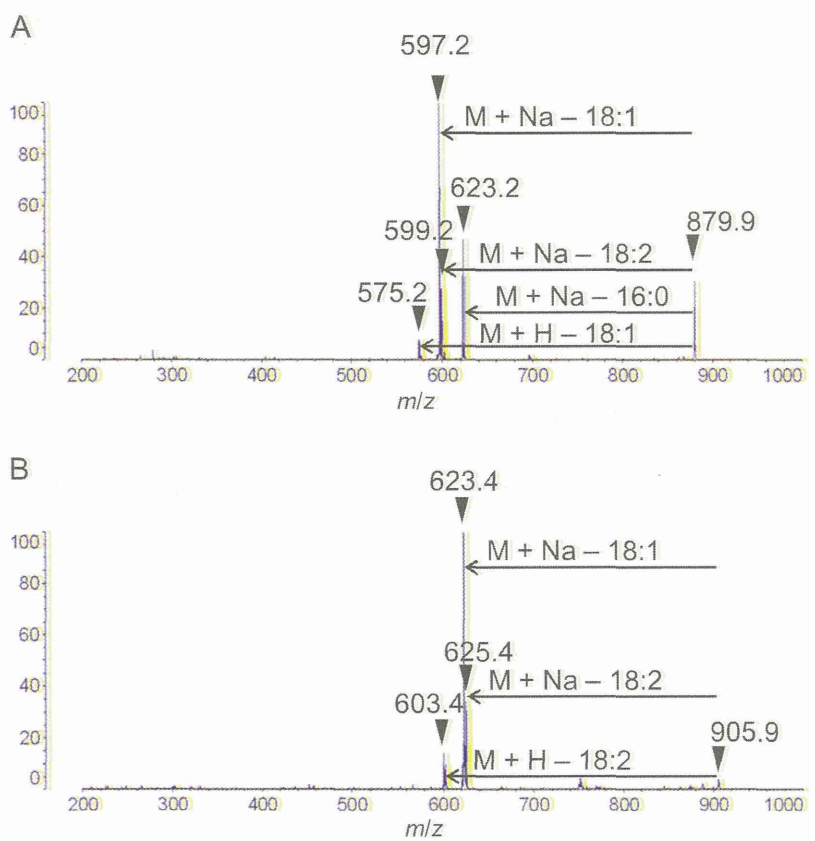

Fig. 2. Two triacylglycerols are present in the renal hilum. The fragmentation patterns of the molecules *m/z* 879.9 (A) and *m/z* 905.9 (B) in tandem MS analysis were involved with the loss of fatty acids and thereby identified as the triacylglycerols [TAG 16:0/18:2/18:1 + Na] + (A) and [TAG 18:1/18:2/18:1 + Na] + (B), respectively.

MS analysis of extracted lipids from kidney homogenates or urine

Approximately, 5 to 10 μl of lipid extracts were dried on ITO slides and coated by spraying the matrix solution. For inferring the adduct ion, 10 mM (final concentration) sodium or potassium acetate was added to extracted samples since excessive sodium or potassium ions have been shown to modify the signal intensity of polar lipids (Sugiura and Setou, 2009). The procedure was performed, as described above.

LC-LTQ-Orbitrap-MS

LC-LTQ-Orbitrap-MS analysis using an Agilent 1200 system was performed to determine the primary structures of the molecules. All procedures were performed in Kazusa DNA Research Institute, Kisarazu, using a detailed protocol, described previously (Iijima et al., 2008). Briefly, the extracted sample reconstituted in methanol was applied to a TSK-GEL Octyl-80Ts (TOSOH Corporation, Tokyo, Japan). Water (solvent A) and acetonitrile (solvent B) were used as the mobile phase with 0.1% v/v formic acid added to both solvents. The gradient program was as follows: 80% B (0 min), 90% B (20 min), 95% B (40 min), 97% B (60 min), 98% B (80 min), 99% B (100 min), 99% B (110 min), 80% B (110.1 min), and 80% B (120 min). The flow rate was set to 0.015 ml/min, and the column oven temperature at 40 °C; 20 μl of each sample was injected.

Data were analyzed with a molecular formula calculation by using the following databases: KEGG (http://www.genome.jp/kegg/), KNApSAcK (http://kanaya.naist.jp/KNApSAcK/), Flavonoid Viewer (http://www.metabolome.jp/software/FlavonoidViewer/), and LIPID MAPS (http://www.lipidmaps.org/). Molecular species were confirmed by tandem MS of selected peaks and by collating each peak's accurate mass measurement with those from the databases.

Results

Molecular distribution of lipids in the HIGA kidney differs from that in the control kidney

Eight mass peaks—*m/z* 792.6, *m/z* 814.6, *m/z* 830.6, *m/z* 840.6, *m/z* 854.6, *m/z* 856.6, *m/z* 880.6, and *m/z* 882.6—were strongly represented in the HIGA kidney (Figs. 1N–U), but not in the control (Figs. 1A–H).However, 2 significant mass peaks, *m/z* 844.6 and *m/z* 868.6, in the peripheral (cortex) area (Figs. 1I, J, V, W) and 2 significant mass peaks, *m/z* 879.9 and *m/z* 905.9, in the hilum area (Figs. 1K, L, X, Y) were observed in both the HIGA and control kidneys.

Two triacylglycerols identified in the hilum

Tandem MS analysis revealed that the fragmentation patterns of the molecules *m/z* 879.9 and *m/z* 905.9 were involved in the loss of fatty acids and were identified as the triacylglycerols (TAGs) [TAG (16:0/18:2/18:1) + Na]+ and [TAG(18:1/18:2/18:1) + Na]+, respectively, by collating them with existing TAGs in the database (Fig. 2).

Several lipids in the cortex are phosphatidylcholines

LC-LTQ-Orbitrap-MS analysis showed that *m/z* 806.57 and *m/z* 830.57 were commonly seen in lipids extracted from Balb/c and HIGA kidneys (Figs. S1A, B). Tandem MS identified these peaks to correspond to [PC(16:0/22:6) + H]+ and [PC(18:2/22:6) + H]+, respectively (Figs. S1C, D). In addition, *m/z* 844.6 and *m/z* 868.6 were estimated to be carrying a potassium ion as the adduct ion (Fig. 3), and thus, were considered to correspond to [PC(16:0/22:6) + K]+ and [PC (18:2/22:6) + K]+, respectively.

HIGA-specific lipids in the tubular lesions are O-phosphatidylcholines that are possibly related to phosphatidylcholines in the cortex area

LC-LTQ-Orbitrap-MS also revealed that *m/z* 792.59 and *m/z* 818.61 were seen specifically in HIGA (Fig. S1B), and tandem MS analysis determined that they corresponded to [PC(O-16:0/22:6) + H]+ and [PC(O-18:1/22:6) + H]+, respectively (Figs. S1E, F). In addition, *m/z* 814.6 and *m/z* 840.6 were estimated to be carrying a sodium ion as an adduct ion, while *m/z* 830.6 was estimated to be carrying a potassium ion (Fig. 3). Accordingly, *m/z* 792.6, *m/z* 814.6, *m/z* 830.6, and *m/z* 840.6 were considered to correspond to [PC(O-16:0/22:6) + H]+, [PC(O-16:0/22:6) + Na]+, [PC(O-16:0/22:6) + K]+, and [PC (O-18:1/22:6) + Na]+, respectively.

LC-LTQ-Orbitrap-MS failed to identify the corresponding molecules of *m/z* 854.6, *m/z* 856.6, *m/z* 880.6, and *m/z* 882.6 because the mass peaks compatible to them were absent; however, the adduct ion of these molecules were speculated to be a sodium ion (Fig. 3). Moreover, the fragmentation patterns analyzed by on-section tandem MS analysis revealed that these molecules possessed a regularity of arrangement and were part of orderly structures (Fig. 4).

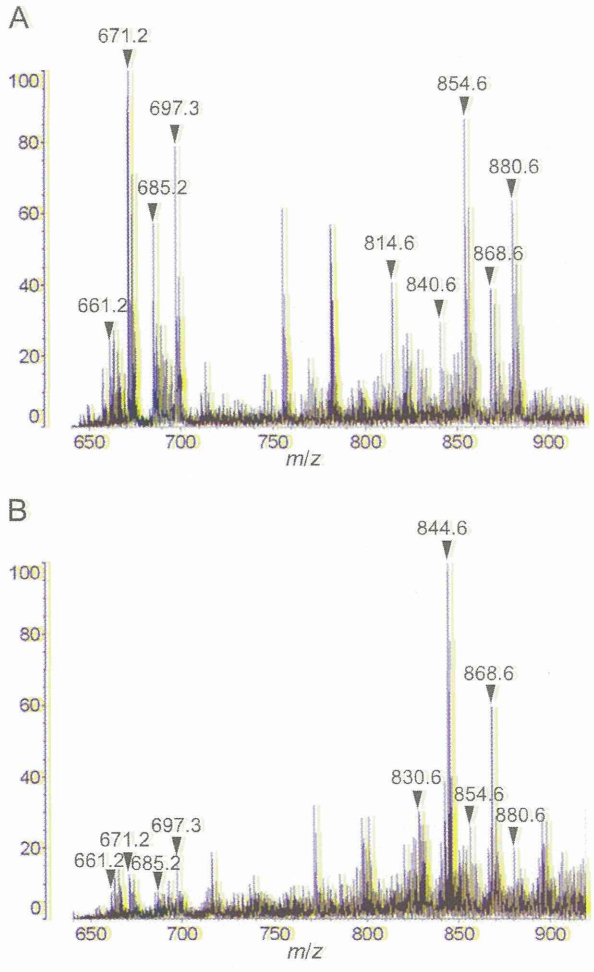

Fig. 3. Addition of sodium or potassium ions in the lipid extracts implied the identity of the adduct ions. The mass peak signals *m/z* 814.6, *m/z* 840.6, *m/z* 854.6, *m/z* 856.6, *m/z* 880.6, and *m/z* 882.6 are intensified when sodium ions are added in the lipid extracts of HIGA kidneys (A); *m/z* 830.6, *m/z* 844.6, and *m/z* 868.6 are intensified when potassium ions are added (B); but *m/z* 792.6 was not intensified in either condition. Thus, these results imply that the adduct ion of *m/z* 814.6, *m/z* 840.6, *m/z* 854.6, *m/z* 856.6, *m/z* 880.6, and *m/z* 882.6 might be sodium, and the adduct ion of *m/z* 830.6, *m/z* 844.6, and *m/z* 868.6 might be potassium.

Urinary stagnation causes HIGA-specific distribution of lipids in the tubular area

For understanding the source from where HIGA-specific molecules were derived, it was important to investigate whether these lipids were excreted in urine. Mass peaks of lipids extracted from urine were investigated using MALDI-QIT-TOF-MS and compared with those from the kidney. The results showed that significant mass peaks in the urine matched the HIGA-specific mass peaks in the kidney (Fig. 5). Thus, we verified that the HIGA-specific molecules were lipids that were normally excreted in urine. We also found that the artificial urinary stagnation due to UUO in Balb/c mice could reproduce the HIGA-specific distribution of lipids in the tubular area (Fig. 6) and that these molecules were, therefore, derived from the urine.

Discussion

We revealed the molecular distribution of lipids in the kidneys, hypothesized on the underlying mechanisms causing the HIGA-specificity, and determined the identity of several molecules by using IMS in combination with LC-LTQ-Orbitrap-MS (Table 1).

We noticed a similarity among PC(16:0/22:6), PC(18:2/22:6), PC(O-16:0/22:6), and PC(O-18:1/22:6) (Fig. 7). All these molecules have 22:6 lipid side chains. Molecules that were common in both the HIGA and normal kidneys were regular PCs and were distributed in the cortex area; while HIGA-specific molecules were O-PCs and distributed in the tubular areas. In addition, the only difference between PC(16:0/22:6) and PC(O-16:0/22:6) was an oxygen atom in the 16:0 side chains. Similarly, the only differences between PC(18:2/22:6) and PC(O-18:1/22:6) were an

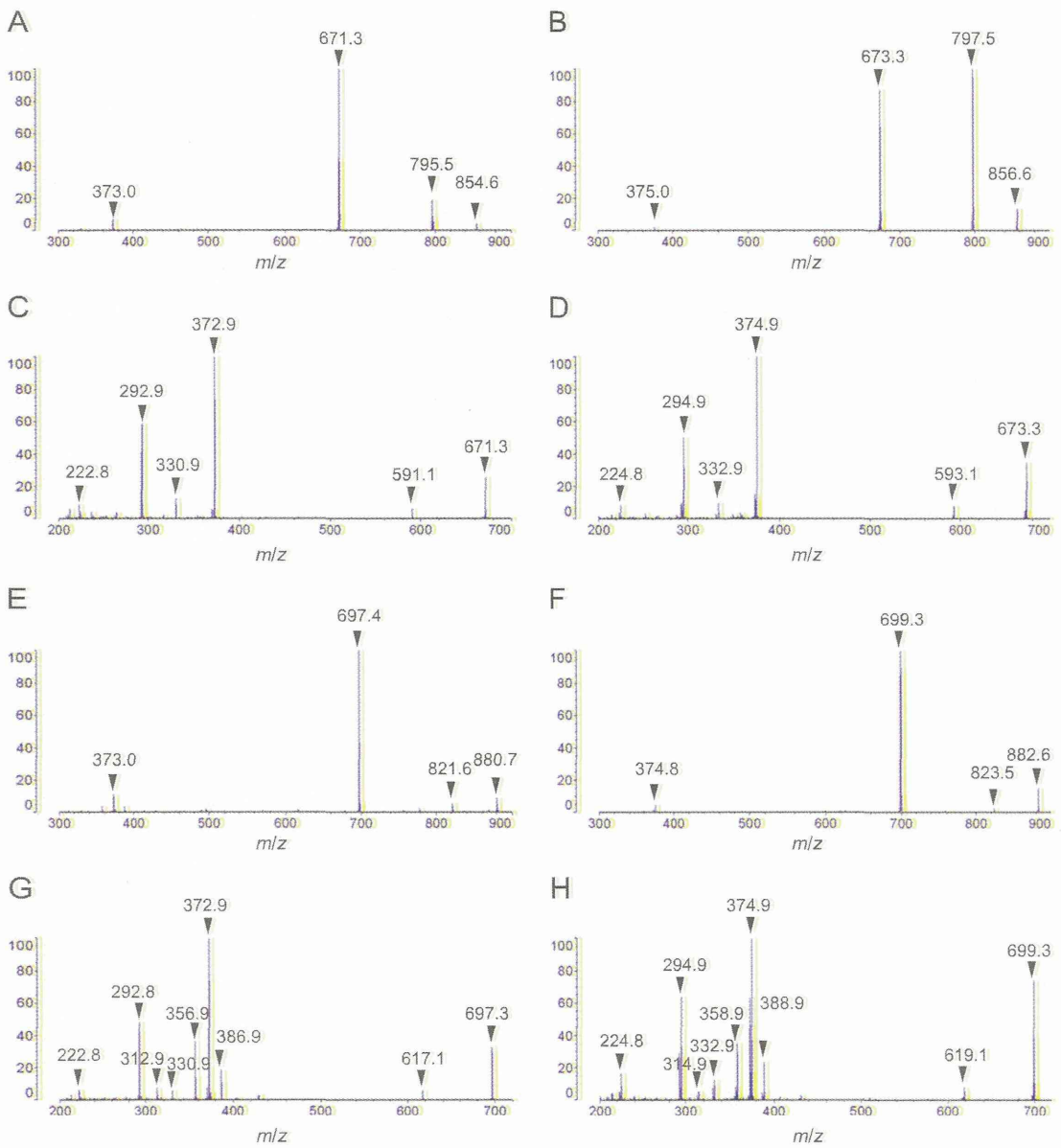

Fig. 4. Tandem MS analysis of HIGA kidney-specific mass peaks *m/z* 854.6, *m/z* 856.6, *m/z* 880.6, and *m/z* 882.6 shows their molecular relationship. The fragmentation patterns of the molecules of *m/z* 854.6, *m/z* 856.6, *m/z* 880.6, and *m/z* 882.6 by MS-MS analysis are involved with the loss of *m/z* 59 Da and *m/z* 183 Da (A,B,E,F). Subsequent MS3 analysis failed to identify these molecules, but the similarity in their fragmentation patterns suggests that they are related molecules (C,D,G,H).

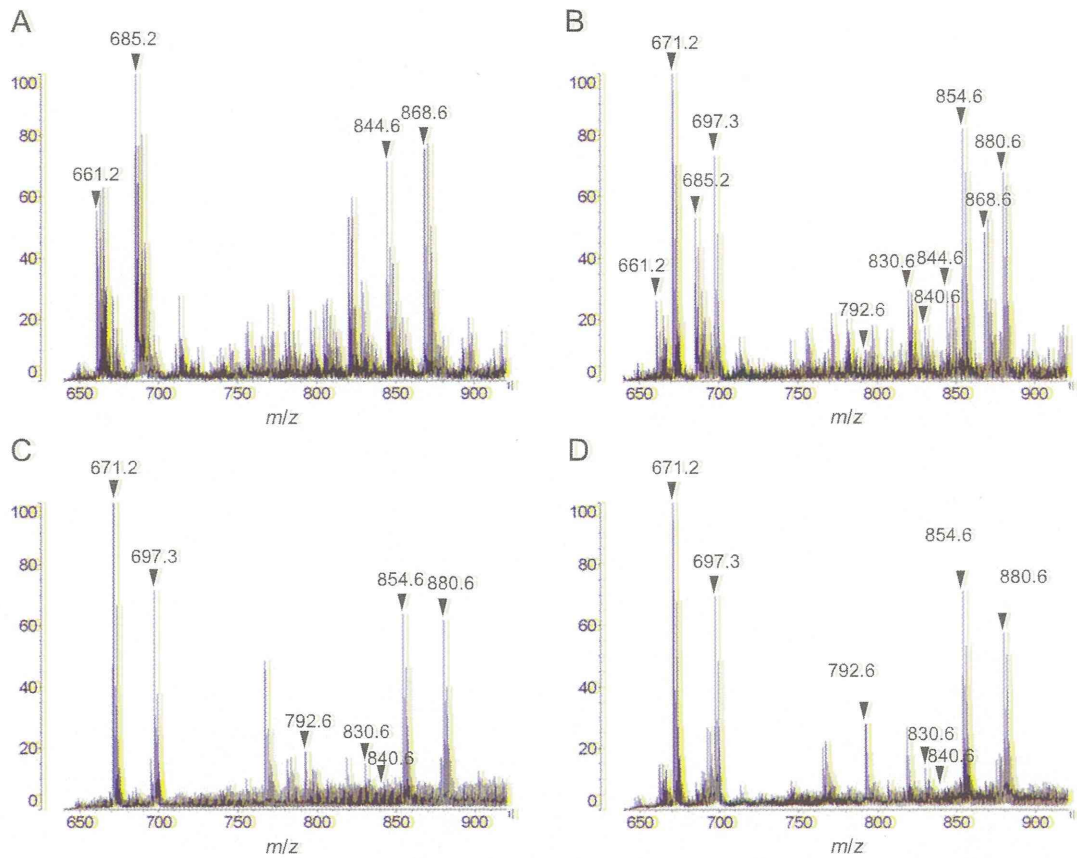

Fig. 5. HIGA-specific lipids are derived from urine. MALDI-QIT-TOF-MS-analyzed mass peaks of lipids extracted from control kidney (A), HIGA kidney (B), control urine (C), and HIGA urine (D) are shown. HIGA-specific mass peaks are seen in both the HIGA and control urine, while the mass peaks that are common in both kidneys are absent in urine.

oxygen atom and a saturation of the side chain. These findings suggest that these molecules may have a novel, unidentified renal function.

Although, we were unable to determine the chemical structures of 4 specific molecules corresponding to *m/z* 854.6, *m/z* 856.6, *m/z* 880.6, and *m/z* 882.6, tandem MS still provided some interesting findings. First, the fragments of *m/z* 854.6 and *m/z* 856.6 always had a difference of 2 Da, which was also true for *m/z* 880.6 and *m/z* 882.6. Second, *m/z* 854.6 and *m/z* 880.6, as well as *m/z* 856 and *m/z* 882 generated several common fragments. Third, PC(O-16:0/22:6) and PC(O-18:1/22:6) had a difference of 26 Da, while *m/z* 854.6 (or *m/z* 856.6) and *m/z* 880.6 (or *m/z* 882.6) also had one. Collectively, the results suggested that these lipids have common structural skeletons. In addition, *m/z* 854.6, *m/z* 856.6, *m/z* 880.6, and *m/z* 882.6 were speculated to be related to PC(O-16:0/22:6) and PC(O-18:1/22:6).

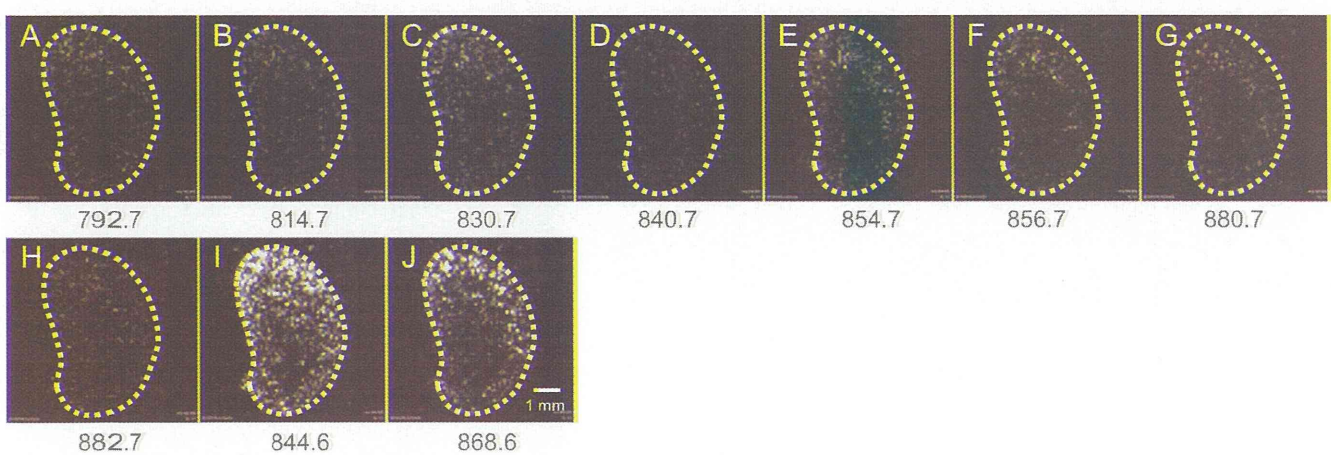

Fig. 6. Artificial urinary stagnation causes HIGA-specific distribution of lipids in tubular area. HIGA-specific mass peaks were detected in the kidneys of a unilateral urethral obstruction model (UUO) in which urine was artificially stagnated (A–H). Images of common mass peaks, *m/z* 844.6 and *m/z* 868.6, are also shown for comparison (I,J). Scale bar indicates a length of 1 mm.

Table 1
Distribution of identified lipid molecules in the kidney.

m/z	Distribution	Specificity	Molecules	Urine
844.6	Cortex	Common	[PC(16:0/22:6)+K]+	
868.6	Cortex	Common	[PC(18:2/22:6)+K]+	
879.7	Hilum	Common	[TAG(16:0/18:2/18:1)+Na]+	
905.9	Hilum	Common	[TAG(18:1/18:2/18:1)+Na]+	
792.6	Medulla	HIGA-specific	[PC(O-16:0/22:6)+H]+	Yes
814.6	Medulla	HIGA-specific	[PC(O-16:0/22:6)+Na]+	Yes
830.6	Medulla	HIGA-specific	[PC(O-16:0/22:6)+K]+	Yes
840.6	Medulla	HIGA-specific	[PC(O-18:1/22:6)+Na]+	Yes
854.6	Medulla	HIGA-specific	Not determined	Yes
856.6	Medulla	HIGA-specific	Not determined	Yes
880.6	Medulla	HIGA-specific	Not determined	Yes
882.6	Medulla	HIGA-specific	Not determined	Yes

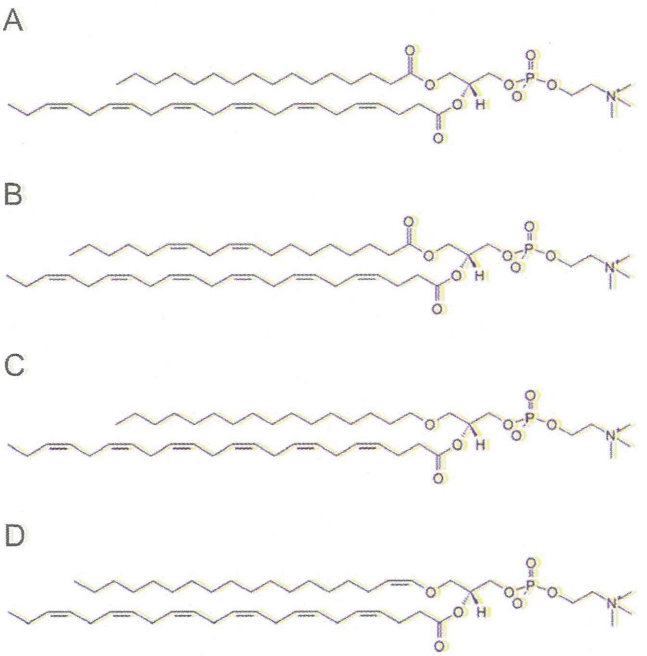

Fig. 7. Phosphatidylcholines that are seen in the control are structurally similar to HIGA-specific O-phosphatidylcholines. Determined or speculated primary structures of selected molecules are shown. Two common phosphatidylcholines that were seen in the cortex area, PC(16:0/22:6) (A) and PC(18:2/22:6) (B), are structurally similar to the HIGA-specific O-phosphatidylcholines, PC(O-16:0/22:6) (C) and PC(O-18:1/22:6), that are seen in the tubular areas and urine (D). The position of the double bonds in the side chains 18:2 and 18:1 were not determined, and therefore the most possible structures, PC(18:2/22:6) and PC(O-18:1/22:6), are shown.

The lesions in the tubular areas of HIGA mouse have been recognized but not well investigated. One of the reasons for this lack of investigation is that the lesions have not been considered a primary defect in IgA nephropathy in human diseases (Coppo et al., 2010). Another reason is absence of a technique that could identify the molecules. In this study, we detected molecular differences between HIGA and Balb/c mice. These findings could be associated with the histological differences that we have already indicated.

We also revealed that HIGA-specific lipids distributed in the tubular area are derived from urine and succeeded in reproducing the same findings by artificial urinary stagnation using the UUO model; this suggests that urinary stagnation causes HIGA-specific distribution. Urinary stagnation seems not to be the primary cause of IgA because it seems unrelated to glomerular lesions. This finding suggests that urinary stagnation and deposition of these molecules in the tubular area could affect the pathogenesis of the nephropathy and could be a clue for understanding other pathologic mechanisms such as acute renal failure.

Although we now have a better understanding of the mechanisms underlying the HIGA-specific molecular distribution of lipids in the kidney, the following issues need to be investigated: determination of the unidentified molecules, understanding the excretion system of lipids in urine, and discovery of the molecular differences in glomerular lesions of IgA nephropathy. Moreover, PC(O-16:0/22:6) and PC(O-18:1/22:6) are also known as analogues of platelet-activating factor (PAF) and a plasmalogen, respectively, and it will be worth investigating whether these molecules are related to the pathogenesis in IgA nephropathy (Coppo et al., 2010; Robinson et al., 1988).

Conclusion

In conclusion, our data are the first report that sheds light on the molecular distribution of lipids in the HIGA mouse kidney. In addition, IMS might provide the dynamic physiological function of kidneys in addition to the distributional information so that it might be applied to understanding the pathophysiology of various diseases.

Supplementary materials related to this article can be found online at doi:10.1016/j.yexmp.2011.07.002.

Conflict of Interest statement

The authors declare that there are no conflicts of interest.

Sources of support

This work was partly supported by grants from the Ministry of Education, Culture, Sports, Science and Technology of Japan (SENTAN to M.S., KAKENHI 20591212 and KAKENHI 20790714); the Ministry of Health, Labour and Welfare of Japan (H20shinkouippan012, H20nanchiippan035, H20shinkouippan015 and H23shinkouippan018); the program of Research on Publicly Essential Drugs and Medical Devices of the Japan Health Science Foundation (KHC3333); and Takeda Science Foundation.

Acknowledgment

We thank Koei Okazaki from Kazusa DNA Research Institute for performing the LC-LTQ-Orbitrap-MS analysis and Ms. Ryoko Yamamoto for excellent experimental assistance.

References

Baronas, E.T., Lee, J.W., Alden, C., Hsieh, F.Y., 2007. Biomarkers to monitor drug-induced phospholipidosis. Toxicol. Appl. Pharmacol. 218, 72–78.
Bligh, E.G., Dyer, W.J., 1959. A rapid method of total lipid extraction and purification. Can. J. Biochem. Physiol. 37, 911–917.
Coppo, R., Fonsato, V., Balegno, S., Ricotti, E., Loiacono, E., Camilla, R., Peruzzi, L., Amore, A., Bussolati, B., Camussi, G., 2010. Aberrantly glycosylated IgA1 induces mesangial cells to produce platelet-activating factor that mediates nephrin loss in cultured podocytes. Kidney Int. 77, 417–427.
Drummond, S.P., Allen, T.D., 2008. From live-cell imaging to scanning electron microscopy (SEM): the use of green fluorescent protein (GFP) as a common label. Methods Cell Biol. 88, 97–108.
Grunkin, M., Raundahl, J., Foged, N.T., 2011. Practical considerations of image analysis and quantification of signal transduction IHC staining. Methods Mol. Biol. 717, 143–154.
Hayasaka, T., Goto-Inoue, N., Sugiura, Y., Zaima, N., Nakanishi, H., Ohishi, K., Nakanishi, S., Naito, T., Taguchi, R., Setou, M., 2008. Matrix-assisted laser desorption/ionization quadrupole ion trap time-of-flight (MALDI-QIT-TOF)-based imaging mass spectrometry reveals a layered distribution of phospholipid molecular species in the mouse retina. Rapid Commun. Mass Spectrom. 22, 3415–3426.
Iijima, Y., Nakamura, Y., Ogata, Y., Tanaka, K., Sakurai, N., Suda, K., Suzuki, T., Suzuki, H., Okazaki, K., Kitayama, M., Kanaya, S., Aoki, K., Shibata, D., 2008. Metabolite annotations based on the integration of mass spectral information. Plant J. 54, 949–962.

Kurashige, T., Abe, K., Furusu, A., Miyazaki, M., Obata, Y., Xia, Z., Nakazawa, M., Nakazawa, Y., Funakoshi, S., Harada, T., Koji, T., Kohno, S., 2008. Renoprotective effect of azelnidipine in rats. Biol. Pharm. Bull. 31, 2237–2244.

Li, L., Zepeda-Orozco, D., Black, R., Lin, F., 2010. Autophagy is a component of epithelial cell fate in obstructive uropathy. Am. J. Pathol. 176, 1767–1778.

Mimura, K., Zhao, B., Muguruma, K., Frenkel, R.A., Johnston, J.M., 1996. Changes in glycerophospholipid profile in experimental nephrotic syndrome. Metabolism 45, 822–826.

Muda, A.O., Feriozzi, S., Rahimi, S., Faraggiana, T., 1995. Spatial arrangement of IgA and C3 as prognostic indicator of IgA nephropathy. J. Pathol. 177, 201–208.

Muso, E., Yoshida, H., Takeuchi, E., Yashiro, M., Matsushima, H., Oyama, A., Suyama, K., Kawamura, T., Kamata, T., Miyawaki, S., Izui, S., Sasayama, S., 1996. Enhanced production of glomerular extracellular matrix in a new mouse strain of high serum IgA ddY mice. Kidney Int. 50, 1946–1957.

Robinson, D.R., Tateno, S., Patel, B., Hirai, A., 1988. Dietary marine lipids after the course of autoimmune disease. Prog. Clin. Biol. Res. 282, 295–303.

Setou, M., Kurabe, N., 2011. Mass microscopy: high-resolution imaging mass spectrometry. J. Electron Microsc. (Tokyo) 60, 47–56.

Sugiura, Y., Setou, M., 2009. Selective imaging of positively charged polar and nonpolar lipids by optimizing matrix solution composition. Rapid Commun. Mass Spectrom. 23, 3269–3278.

Willems, S.M., van Remoortere, A., van Zeijl, R., Deelder, A.M., McDonnell, L.A., Hogendoorn, P.C., 2010. Imaging mass spectrometry of myxoid sarcomas identifies proteins and lipids specific to tumour type and grade, and reveals biochemical intratumour heterogeneity. J. Pathol. 222, 400–409.

Yasuda, Y., Cohen, C.D., Henger, A., Kretzler, M., 2006. The European Renal cDNA Bank (ERCB) Consortium: Gene expression profiling analysis in nephrology: towards molecular definition of renal disease. Clin. Exp. Nephrol. 10, 91–98.

Yoshioka, Y., Tsutsumi, T., Adachi, M., Tokumura, A., 2009. Altered phospholipid profile in urine of rats with unilateral ureteral obstruction. Metabolomics 5, 429–433.

Zhang, H., Saha, J., Byun, J., Schin, M., Lorenz, M., Kennedy, R.T., Kretzler, M., Feldman, E.L., Pennathur, S., Brosius III, F.C., 2008. Rosiglitazone reduces renal and plasma markers of oxidative injury and reverses urinary metabolite abnormalities in the amelioration of diabetic nephropathy. Am. J. Physiol. Renal Physiol. 295, F1071–F1081.

Anal Bioanal Chem (2011) 400:1895–1904
DOI 10.1007/s00216-011-4895-5

ORIGINAL PAPER

Semi-quantitative analyses of metabolic systems of human colon cancer metastatic xenografts in livers of superimmunodeficient NOG mice

Akiko Kubo · Mitsuyo Ohmura · Masatoshi Wakui · Takahiro Harada · Shigeki Kajihara · Kiyoshi Ogawa · Hiroshi Suemizu · Masato Nakamura · Mitsutoshi Setou · Makoto Suematsu

Received: 29 November 2010 / Revised: 7 February 2011 / Accepted: 9 March 2011 / Published online: 10 April 2011

Abstract Analyses of energy metabolism in human cancer have been difficult because of rapid turnover of the metabolites and difficulties in reducing time for collecting clinical samples under surgical procedures. Utilization of xenograft transplantation of human-derived colon cancer HCT116 cells in spleens of superimmunodeficient NOD/SCID/IL-2Rγ^{null} (NOG) mice led us to establish an experimental model of hepatic micrometastasis of the solid tumor, whereby analyses of the tissue sections collected by snap-frozen procedures through newly developed microscopic imaging mass spectrometry (MIMS) revealed distinct spatial distribution of a variety of metabolites. To perform intergroup comparison of the signal intensities of metabolites among different tissue sections collected from mice in fed states, we combined matrix-assisted laser desorption/ionization time-of-flight imaging mass spectrometry (MALDI–TOF-IMS) and capillary electrophoresis–mass spectrometry (CE–MS), to determine the apparent contents of individual metabolites in serial tissue sections. The results indicated significant elevation of ATP and energy charge in both

The first two authors equally contributed to this work.

Published in the special issue *Biomedical Mass Spectrometry* with Guest Editors Hisao Oka and Mitsutoshi Setou.

Electronic supplementary material The online version of this article (doi:10.1007/s00216-011-4895-5) contains supplementary material, which is available to authorized users.

A. Kubo · M. Ohmura · M. Suematsu
Department of Biochemistry, School of Medicine,
Keio University,
35 Shinanomachi, Shinjuku-ku,
Tokyo 160–8582, Japan

M. Ohmura · M. Suematsu (✉)
Japan Science and Technology Agency (JST),
Exploratory Research for Advanced Technology
(ERATO) Suematsu Gas Biology Project,
35 Shinanomachi, Shinjuku-ku,
Tokyo 160–8582, Japan
e-mail: msuem@sc.itc.keio.ac.jp

M. Wakui
Department of Laboratory Medicine,
School of Medicine,
Keio University,
35 Shinanomachi, Shinjuku-ku,
Tokyo 160–8582, Japan

T. Harada · S. Kajihara · K. Ogawa
Technology Research Laboratory, Shimadzu Corporation,
3-9-4 Hikaridai, Seika-cho, Soraku-gun,
Kyoto 619–0237, Japan

H. Suemizu · M. Nakamura
Central Institute for Experimental Animals,
1430 Nogawa, Miyamae-ku, Kawasaki-shi,
Kanagawa 216–0001, Japan

M. Nakamura
Department of Pathology and Regenerative Medicine,
Tokai University School of Medicine,
143 Shimokasuya, Isehara-shi,
Kanagawa 259–1193, Japan

M. Setou
Department of Molecular Anatomy,
Molecular Imaging Frontier Research Center,
Hamamatsu University School of Medicine,
1-20-1 Handayama, Higashi-ku, Hamamatsu-shi,
Shizuoka 431–3192, Japan

metastases and the parenchyma of the tumor-bearing livers. To note were significant increases in UDP-*N*-acetyl hexosamines, and reduced and oxidized forms of glutathione in the metastatic foci versus the liver parenchyma. These findings thus provided a potentially important method for characterizing the properties of metabolic systems of human-derived cancer and the host tissues in vivo.

Keywords Imaging mass spectrometry (IMS) · Matrix-assisted laser desorption/ionization (MALDI) · Capillary electrophoresis–mass spectrometry (CE–MS) · Tumor-bearing liver · Metabolome · Glycoprotein biosynthesis

Abbreviations

CE–MS	capillary electrophoresis–mass spectrometry
MALDI	matrix assisted laser desorption/ionization

Introduction

Imaging mass spectrometry (IMS) has enabled us to collect spatial information about a variety of biomolecules, for example phospholipids [1, 2], drugs [3], peptides [4, 5], and metabolites [6–8] in tissue sections in situ. Many kinds of ion sources for imaging mass spectrometry had been developed in recent years. For example, ultraviolet matrix-assisted laser desorption/ionization (MALDI) is capable of producing ions from low-molecular-mass compounds, being promising for imaging volatile compounds in fresh ginger samples [9]. Low-molecular-mass metabolites have also been analyzed by other methods including desorption electrospray ionization and desorption/ionization on silicon [10, 11]. In these methods, samples should be dried before image acquisition of metabolomic snapshots to avoid enzymatic degradation of the molecule of interest. On the other hand, laser ablation electrospray ionization or infrared MALDI are other useful methods of molecular imaging that are applicable to water-rich specimens to ionize the analytes [12, 13].

In order to acquire reliable images of metabolites in and around cancers in vivo, several lines of methodological consideration are necessary. First, enzymatic reactions in tissue and cell samples should be terminated as soon as possible. Second, soft ionization of the molecules seemed desirable to identify individual peaks of metabolites. Finally, high spatial resolution at cellular levels is required to examine differences in metabolic properties between the cancer foci and the surrounding host tissues. In this context, application of ultraviolet MALDI to freeze-dried tissue samples is suitable for examining cancer metabolism in vivo. Regarding the spatial resolution of the ultraviolet MALDI, the raster scan pitch of the laser application has been restricted by its focusing diameter, in the approximate range 50–200 μm [7, 8]. Our newly developed UV–MALDI–quadrupole ion-trap (QIT)-TOF-MS instrument, that is, a mass microscope with 10-μm spatial resolution, overcame this problem of spatial resolution by improvement of the ion source to control the position of the sample stage three-dimensionally with high accuracy [9, 14, 15]. Using 9-aminoacridine as a matrix, metabolites, such as high-energy nucleotides and phosphorylated carbohydrates became directly detectable in frozen tissue sections [6]. Since then, various types of tissues including brain and muscles of mice have been analyzed experimentally to dissect molecular mechanisms for metabolic systems in vivo [7, 8, 16].

The objective of this study was to characterize metabolic systems in and around human-derived solid tumors in vivo. Although distinct properties of cancer metabolism known as Warburg effects have been examined mainly in cultured systems or conventional animal experiments, there are several technical difficulties in characterizing the metabolism of human solid tumors in vivo. First, it is difficult to shorten the time for sampling of tissues to avoid degradation of metabolites with rapid turnover under surgical procedures. Second, because of large variances of the mass intensities of molecules among individual tissue samples, a method to semi-quantify their signals and to compare these among individual samples should be developed. To overcome the first problem, we have herein utilized an experimental model of xenograft transplantation of human-derived colon cancer HCT 116 cell line in superimmunodeficient NOD/SCID/IL-2Rγ^{null} (NOG) mice [17]. In this model, we were able to collect snap-frozen samples of the tumor-bearing liver for analyses by using imaging mass spectrometry with high spatial resolution. To solve the second problem, we used serial sections of the liver to determine total amounts of individual metabolites, using CE–MS for data calibration. This method enabled us to carry out intergroup comparison of semi-quantitative metabolite data in and around micrometastases of the human-derived colon cancer. Results obtained in this study revealed that the tumor-bearing liver accelerates its energy metabolism. Furthermore, several metabolites including UDP-*N*-acetyl hexosamine (UDP-HexNAc) and glutathione, and the value of energy charge were significantly elevated in the metastatic foci, suggesting significance of these molecules as marker metabolites enriched in the cancer in vivo.

Experimental

Chemicals

9-Aminoacridine (9-AA) was purchased from Merck Schuchardt (Hohenbrunn, Germany). All chemical stan-